Phlorizin ameliorates myocardial fibrosis by inhibiting pyroptosis through restraining HK1-mediated NLRP3 inflammasome activation

Yuling Zhang [a,1], Xizhen Cheng [a,1], Yanan Wang [a], Haochuan Guo [a], Yongxing Song [a,c,**], Hongfang Wang [a,b,***], Donglai Ma [a,b,c,*]

[a] School of Pharmacy, Hebei University of Chinese Medicine, Shijiazhuang, 050200, Hebei, China
[b] Hebei Technology Innovation Center of TCM Formula Preparations, Shijiazhuang, 050200, Hebei, China
[c] Traditional Chinese Medicine Processing Technology Innovation Center of Hebei Province, Shijiazhuang, 050091, Hebei, China

ARTICLE INFO

ABSTRACT

The specific role of phlorizin (PHL), which has antioxidant, anti-inflammatory, hypoglycemic, antiarrhythmic and antiaging effects, on myocardial fibrosis (MF) and the related pharmacological mechanisms remain unknown. The objective of this study was to determine the protective actions of PHL on isoprenaline (ISO)-induced MF and its molecular mechanisms in mice. PHL was administered at 100 and 200 mg/kg for 15 consecutive days with a subcutaneous injection of ISO (10 mg/kg). MF was induced by ISO and alleviated by treatment with PHL, as shown by reduced fibrin accumulation in the myocardial interstitium and decreased levels of myocardial enzymes, such as creatinine kinase-MB, lactate dehydrogenase, and aspartate transaminase. In addition, PHL significantly decreased the expression of the fibrosis-related factors alpha smooth muscle actin, collagen I, and collagen III induced by ISO. The generation of intracellular reactive oxygen species induced by ISO was attenuated after PHL treatment. The malondialdehyde level was reduced, whereas the levels of superoxide dismutase, catalase, and glutathione were elevated with PHL administration. Moreover, compared to ISO, the level of Bcl-2 was increased and the level of Bax protein was decreased in the PHL groups. PHL relieved elevated TNF-α, IL-1β, and IL-18 levels as well as cardiac mitochondrial damage resulting from ISO. Further studies showed that PHL downregulated the high expression of hexokinase 1 (HK1), NLRP3, ASC, Caspase-1, and GSDMD-N caused by ISO. In conclusion, our findings suggest that PHL protects against ISO-induced MF due to its antioxidant, anti-apoptotic, and anti-inflammatory activities and via inhibition of pyroptosis mediated by the HK1/NLRP3 signaling pathway *in vivo*.

1. Introduction

Myocardial fibrosis (MF), the result of the deposition of extracellular matrix proteins, develops as a consequence of many different

myocardial conditions, including myocardial infarction (MI), hypertension, and myocarditis [1]. MF can result in serious complications, such as cardiac hypertrophy, which lead to decreased ventricular wall compliance and limited ventricular activity and induce arrhythmias and even sudden death. It has increasingly become a prominent public health problem worldwide [2]. Therefore, improving MF is a key therapeutic target in the clinical treatment of various heart diseases.

MF is commonly associated with an augmented inflammatory response, and pyroptosis represents a form of programmed cell death that triggers the release of pro-inflammatory cytokines, thereby promoting collagen deposition and accelerating cardiac fibrosis production [3]. Oxidative stress is involved in a variety of systemic diseases, including MF [4]. The accumulation of mitochondrial reactive oxygen species (ROS) is involved in mitochondrial dysfunction and subsequent activation of apoptosis and the NLRP3 inflammasome in cardiac injury [5,6]. To protect the heart from damage, inhibiting the mitochondria-dependent apoptosis of cardiomyocytes under oxidative stress is critical [7]. The NLRP3 inflammasome is a multiprotein complex consisting of the sensor molecule NLRP3, ASC, and pro-caspase-1, which mediates the stimulation of Caspase-1 [8]. Activated Caspase-1 cleaves Gasdermin D (GSDMD) to release GSDMD-N, which can form pores causing the excretion of mature interleukin 1 beta (IL-1β) and IL-18, and then triggering pyroptosis in heart diseases [9,10].

Hexokinase 1 (HK1) is an essential factor in the regulation of NLRP3 inflammasome activation [11]. HK1 is the key rate-limiting enzyme responsible for the first reaction in glycolysis, which is located in the cytoplasm and is overexpressed in many inflammatory responses [12,13]. The downregulation of HK1-dependent glycolysis regulates NLRP3 inflammasome activation in atherosclerosis, whose pathogenesis may be to protect vascular endothelial cells against pyroptosis [14]. This indicates that HK1 may play an important role in cardiovascular disease.

Phlorizin (PHL, $C_{21}H_{24}O_{10}$, Fig. 1), a major dihydrochalcone derived from apples, has antioxidant, anti-inflammatory, and anti-tumor properties [15,16]. The administration of apple polyphenol extract ameliorates acute ulcerative colitis by inhibiting pyroptosis [17]. PHL protects against arrhythmias by ameliorating the slowing of pulse conduction during ischemia [18]. PHL can modulate cardiac lipid and energy metabolism to mitigate diabetic cardiomyopathy [19]. These studies indicate that PHL may play a cardioprotective role during disease development; however, the detailed mechanisms underlying the anti-myocardial fibrotic effects of PHL are unclear.

Isoproterenol (ISO) is commonly used to establish animal models of myocardial ischemia and MF [20,21]. This study researched whether the mechanism underlying the anti-MF effects of PHL is based on inhibiting pyroptosis by restraining HK1-mediated NLRP3 inflammasome activation, which will provide evidence for clinical application.

2. Methods

2.1. Drugs

PHL (purity >98 %) was purchased from Shanghai Yuanye Bio-Technology Co., Ltd. (Shanghai, China). The PHL was suspended in 0.5 % carboxymethylcellulose sodium (0.5 % CMC-Na) and stored at room temperature. ISO was purchased from Sigma–Aldrich (St. Louis, MO, USA) and dissolved in normal saline after adding 5 % dimethyl sulfoxide.

2.2. Animals

A total of 50 male Kunming mice (6–8 weeks old, 17–20 g) were purchased from Liaoning Changsheng Biotechnology Co., Ltd. And remained in an animal facility (23 ± 2 °C; 45–60 % relative humidity) with adequate food and water under a 12 h light/dark cycle. This research was approved by the Medical Ethics Committee of Hebei University of Chinese Medicine (Certificate No. DWLL2021107, Hebei Province, China).
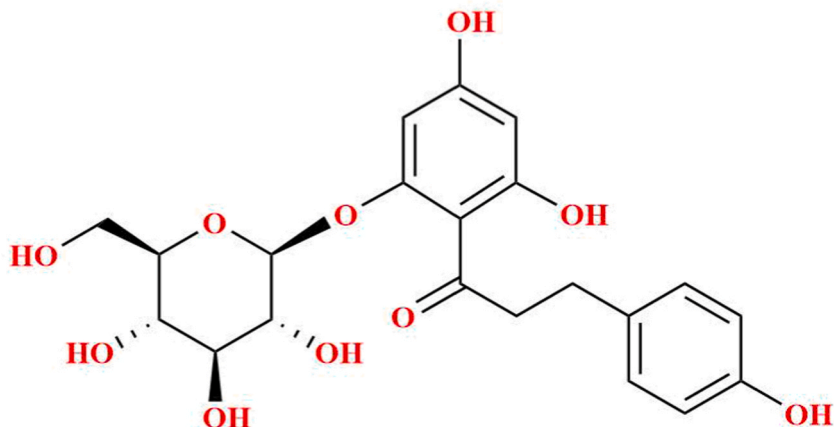

Fig. 1. Chemical structure of phlorizin (PHL).

2.3. Experimental design

The 50 mice were fed water freely for a 7-day adaptation period and then divided into the following five groups at random (n = 10 each group).

① control group (CONT): 0.5 % CMC-Na (intragastric (i.g.)) + NS (subcutaneous (s.c.)).
② model group (ISO): 0.5 % CMC-Na i. g.) + ISO 10 mg/kg/day (s.c.).
③ low-dose drug intervention group (PHL-L + ISO): PHL 100 mg/kg (i.g.) + ISO 10 mg/kg (s.c.).
④ high-dose drug intervention group (PHL-H + ISO): PHL 200 mg/kg (i.g.) + ISO 10 mg/kg (s.c.).
⑤ single-dose drug intervention group (PHL): PHL 200 mg/kg (i.g.) + NS (s.c.).

The dose choice of ISO and PHL was based on previous studies [22,23]. All of the drugs were administered once a day for 14 days, and all of the mice were anesthetized with thiopentone (35 mg/kg, intraperitoneal (i.p.)) after fasting from water for 24 h. Blood samples were obtained from the retro-orbital venous plexus. The supernatant was extracted after centrifuging at 3500 rpm for 10 min and stored at $-20\,^\circ$C for subsequent testing. Additionally, the heart tissue (approximately 1 mm^3) was removed from the same location of the apex of the heart and then immediately immersed in 2.5 % glutaraldehyde phosphate buffer to observe the ultrastructure of the mitochondria. The remaining heart was cut in half: one half was fixed in 4 % paraformaldehyde for 24 h to observe the histopathology, and the other half was stored at $-80\,^\circ$C for enzyme-linked immunoassay (ELISA), fluorescence microscopy, and Western blot analyses.

2.4. Morphological detection of the heart

The cardiac tissues fixed in 4 % paraformaldehyde for 1 week were embedded in paraffin wax and then cut into 4 µm sections. Hematoxylin and eosin (H&E) and Masson's trichrome staining were performed consistently in the commercial illustration to observe histopathological changes and collagen deposition. After the sections were dehydrated, made transparent, and sealed, the images were captured with an optical microscope (DM4000B, Leica, Solms, Germany).

2.5. Serum biochemical analysis

The supernatant was used to measure the cardiac injury marker levels in accordance with the handbooks of available kits. Cardiac troponin I (cTnI), creatine kinase-MB (CK-MB), lactate dehydrogenase (LDH), and aspartate aminotransferase (AST) were detected with the cTnI ELISA Kit (SEKM-0153, Sigma) and CK-MB, LDH, and AST kits (GM1122, GM1120 and GM1103, respectively; Wuhan Saipei Biotechnology Co., Ltd., Wuhan, China).

2.6. Biochemical index analysis

At 4 $^\circ$C, the cardiac tissue was prepared in a 10 % homogenate solution and centrifuged at 12,000 rpm for 5 min twice to obtain the supernatants. Superoxide dismutase (SOD, A001-1), malondialdehyde (MDA, A003-1), glutathione (GSH, A006-2), and catalase (CAT, A007-2) levels were determined using manufacturers' kits (Jiancheng, Nanjing, China) according to the instructions.

2.7. ROS generation analysis

ROS generation was estimated with dihydroethidium (DHE) (G1706, Servicebio, China) fluorescence. Briefly, fresh heart tissue was sectioned with a frozen slicer and cut into 6 µm sections. The heart tissues were loaded with 10 µM DHE for 30 min, incubated with DAPI staining solution (G1012, Servicebio) for 10 min in the dark, and then washed with PBS. The intensity of fluorescence was observed with an inverted fluorescence microscope (DM4000B, Leica) to evaluate ROS generation.

2.8. Mitochondrial ultrastructure analysis

After soaking in 2.5 % glutaraldehyde phosphate buffer at 4 $^\circ$C for 2.5 h, the cardiac tissues were fixed in 1 % osmic acid with 0.1 mol/L phosphate buffer (pH 7.4) at 25 $^\circ$C for 2 h. Then, the tissues were dehydrated, immersed, embedded, and sliced into ultrathin sections. Next, the sections were dyed using 2 % uranyl acetate saturated alcohol solution and lead citrate. Finally, the mitochondrial ultrastructure was captured by transmission electron microscopy (TEM) (ZOOM-1 HC-1, Hitachi, Tokyo, Japan) at 80.0 kV.

2.9. Inflammation-related factor analysis

The levels of inflammation-related factors in tissues were evaluated with the Mouse TNF-α Uncoated ELISA Kit (88–7324, Thermo Fisher Scientific, Waltham, MA, USA), Mouse IL-1β ELISA Kit (SP12667, Wuhan Saipei Biotechnology Co., Ltd., Wuhan, China), and Mouse IL-18 ELISA Kit (EK218-03, Multi Sciences, Hangzhou, China) in line with the manufacturers' guidelines.

2.10. Western blot analysis

The cardiac tissue was chopped and homogenized in RIPA lysis buffer (G2002, Servicebio), and the cardiac tissue homogenate was centrifuged at 4 °C to obtain the protein. Then, equivalent protein samples were separated using 10 % sodium dodecyl sulfate-gel electrophoresis and transferred to polyvinylidene difluoride membranes, followed by blocking in 5 % skimmed milk powder for 2 h. Anti-GAPDH (1:2000, GB15002, Servicebio; and 1:5000, AB0037, Abways, only anti-GSDMD-N) was used as the internal standard. Afterward, the membranes were incubated overnight at 4 °C with the following primary antibodies (1:1000 dilution): anti-alpha smooth muscle actin (α-SMA) (GB111364, Servicebio), anti-collagen I (GB11022, Servicebio), anti-collagen III (GB11023, Servicebio), anti-Bcl-2 (GB113375, Servicebio), anti-Bax (GB12690, Servicebio), anti-Caspase-3 (GB11767C, Servicebio), anti-HK1 (AF1726, Beyotime, Beijing, China), anti-NLRP3 (DF7502, Affinity Biosciences, Cincinnati, OH, USA), anti-ASC (BS-6741R, Bioss Antibodies, Woburn, MA, USA), anti-Caspase-1 (GB11383, Servicebio), and anti-GSDMD-N (ab219800, Abcam). The next day, the membranes were incubated for 1 h under a light-avoiding environment with goat anti-mouse IgG or goat anti-rabbit IgG secondary antibodies (1:5000, GB25301 and GB23303, respectively, both from Servicebio). Alpha Innotech software (alphaEaseFC, Alpha Innotech, America) was applied to analyze the gray value of the target bands and calculate the gray value ratio of the above proteins and GAPDH.

2.11. Statistical analyses

All experimental data are expressed as the mean ± standard error of the mean (SEM). Origin 8.0.2 software (GraphPad Software, America) was used for statistical analyses. The data were first analyzed for normality and homogeneity of variance. Then, one-way analysis of variance and Tukey's post-hoc test were used to evaluate the differences among the five groups, and $p < 0.05$ was considered to be statistically significant.

3. Results

3.1. PHL reduces the extent of MF and the level of fibrosis-related factors in mice

As shown in the H&E staining images, the structure of myocardial tissue in the CONT and PHL groups was clear, the cardiomyocytes were normally arranged, and cardiomyocyte apoptosis, inflammatory cell infiltration, or cardiac fibroblasts were not present (Fig. 2A). Compared to the CONT group, the ISO group displayed disorder of myocardial tissue structure and cardiomyocyte injury, such as cell apoptosis, cell nuclear condensation, inflammatory cell infiltration, and cellular swelling. The latter two pathologic changes were associated with pyroptosis of cardiomyocytes closely. And the histological changes were alleviated in the PHL treatment groups compared with the ISO group (Fig. 2B, $p < 0.01$).

As shown in the masson's trichome staining images, there were massive collagen fibers in the ISO group, while the PHL treatment groups had reduced fibers (Fig. 3A). These histopathologic damage changes were alleviated in the PHL-L + ISO and PHL-H + ISO groups in a dose-dependent manner compared to the ISO group, which illustrated that PHL treatment improved the extent of pathological injury in mice.

The levels of the fibrosis-related factors α-SMA (Fig. 3C), Collagen I (Fig. 3D) and Collagen III (Fig. 3E) in the ISO group were higher
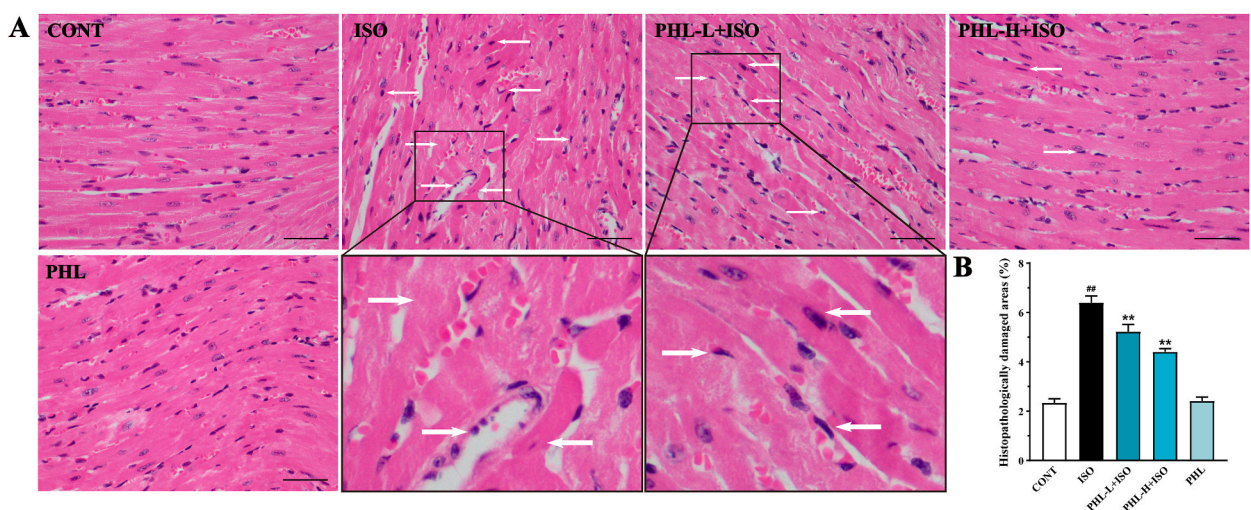

Fig. 2. The effects of PHL on cardiac histopathological changes in ISO-induced mice H&E staining images and arrows represent cell apoptosis, cell nuclear condensation, inflammatory cell infiltration, and cellular swelling (A). The staining is shown for the CONT, ISO, PHL-L + ISO, PHL-H + ISO, and PHL groups (scale bar: 50 μm, × 400). The area of myocardial injury in each group was calculated (B). Data are shown as the mean ± SEM (n = 3). ##$p < 0.01$ vs. CONT group; **$p < 0.01$, *$p < 0.05$ vs. ISO group.
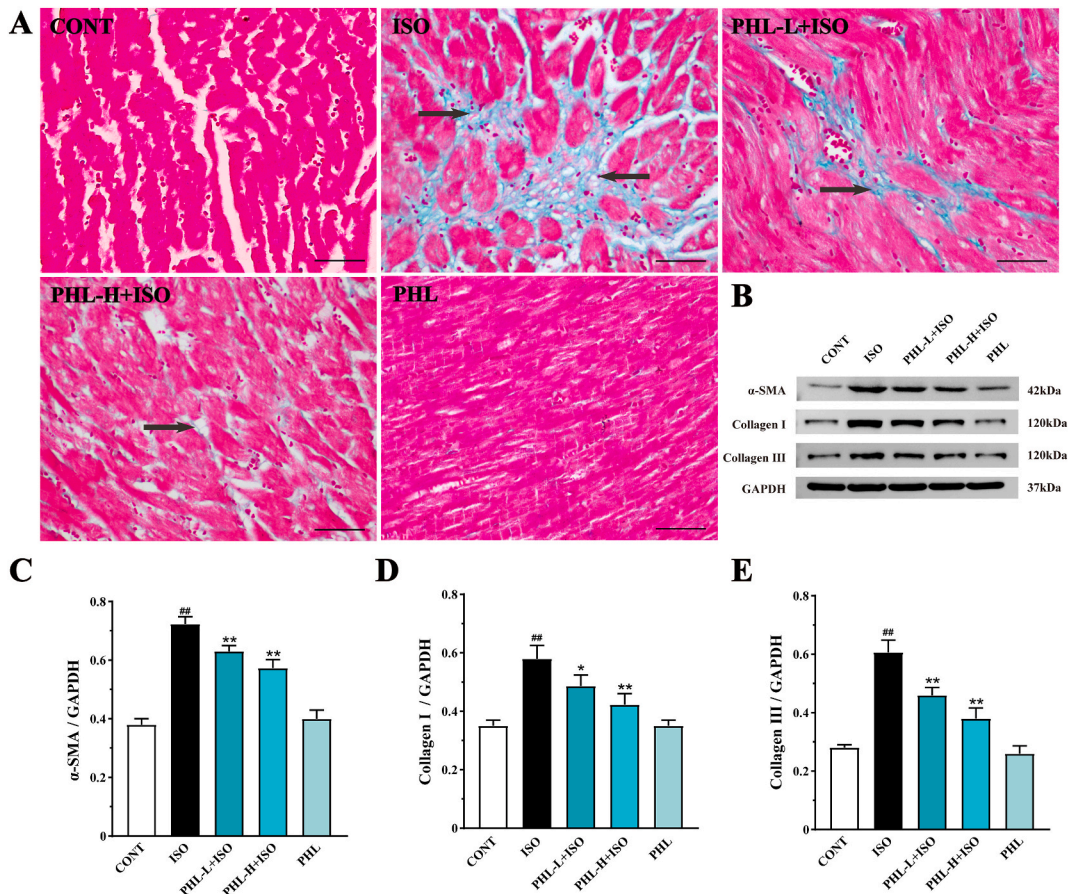
Fig. 3. The effects of PHL on myocardial fibrosis as surveyed by Masson's trichrome staining images and arrows represent collagen fibers (A). The staining is shown for the CONT, ISO, PHL-L + ISO, PHL-H + ISO, and PHL groups (scale bar: 50 μm, × 400). The effects of PHL on the levels of the fibrosis-related factors α-SMA (C), Collagen I (D), and Collagen III (E) in ISO-induced mice (B). Data are shown as the mean ± SEM (n = 3). ##$p <$ 0.01 vs. CONT group; **$p <$ 0.01, *$p <$ 0.05 vs. ISO group.

than those in the CONT group ($p < 0.01$), whereas their expression in the PHL group was lower than that in the ISO group ($p < 0.01$, $p < 0.05$). These results indicated that PHL could decrease the extent of MF and the levels of fibrosis-related factors in mice (Fig. 3B).

3.2. PHL decreases the serum levels of myocardial enzymes

Myocardial enzymes were increased in the ISO group compared with the CONT group ($p < 0.01$), including cTnI (Fig. 4A), CK-MB (Fig. 4B), LDH (Fig. 4C), and AST (Fig. 4D). Compared to the ISO group, myocardial enzymes in the PHL-L + ISO and PHL-H + ISO groups were decreased ($p < 0.01$, $p < 0.05$), whereas the PHL group had no remarkable difference compared with the CONT group.

3.3. PHL effects on oxidative and antioxidant markers

The cardiac tissue biochemical analyses indicated that the ISO group had obviously decreased SOD (Fig. 5A), GSH (Fig. 5C), and CAT (Fig. 5D) expression and increased MDA content (Fig. 5B) compared with the CONT group ($p < 0.01$). PHL treatment improved the expression of SOD, GSH, and CAT ($p < 0.01$, $p < 0.05$) and reduced the level of MDA ($p < 0.01$).

3.4. PHL inhibits ISO-induced ROS generation

As shown in Fig. 6, ROS fluorescence intensity was markedly higher in the ISO group than in the CONT group ($p < 0.01$), whereas that of the PHL-L + ISO treatment groups was clearly lower than that of the ISO group ($p < 0.01$). Detection of ROS generation indicated that PHL inhibited ISO-induced ROS production but had no effect on ROS generation in ISO-defects.
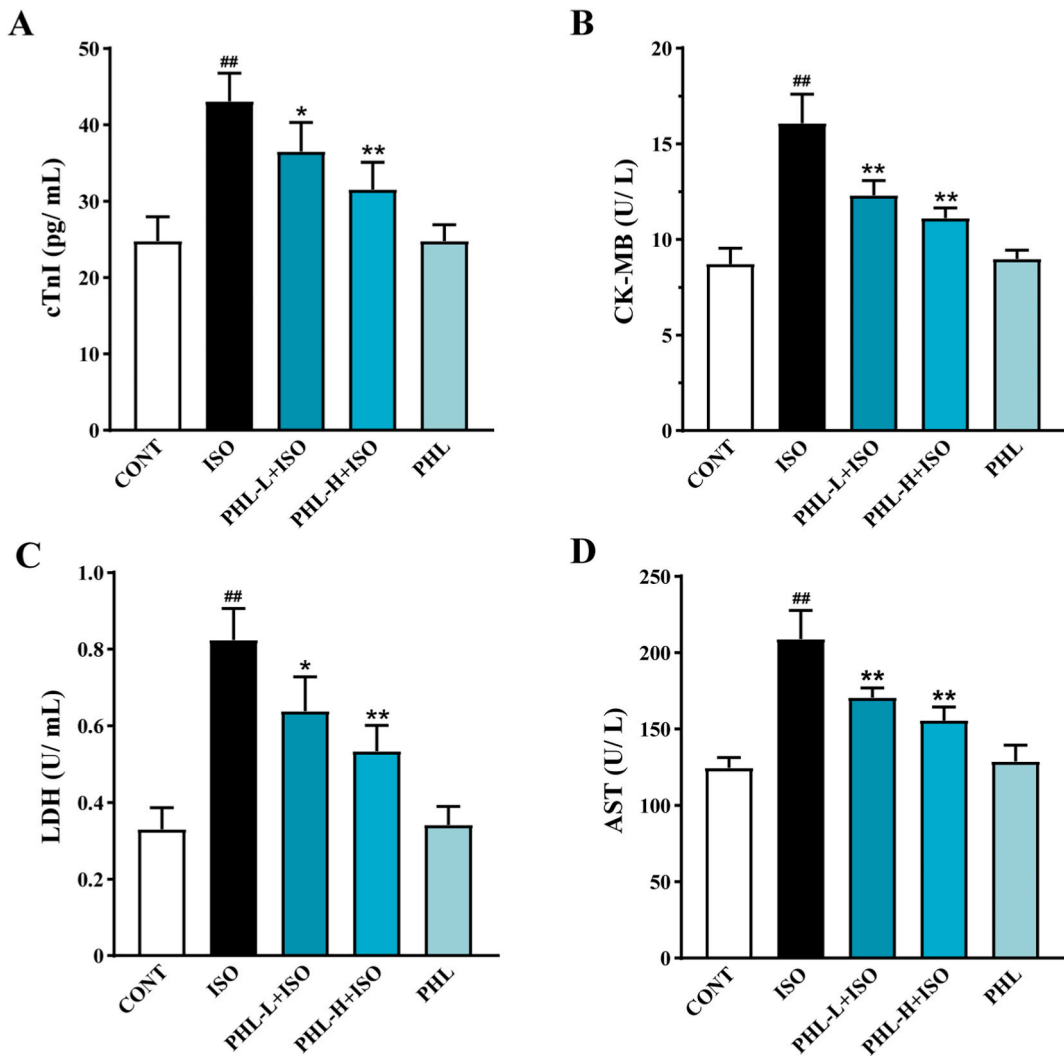
Fig. 4. Expression of cTnI (A), CK-MB (B), LDH (C) and AST (D) are shown between the ISO group and PHL treatment groups. Data are shown as the mean $\pm$ SEM (n = 6). $\#\#p < 0.01$ vs. CONT group; $**p < 0.01$, $*p < 0.05$ vs. ISO group.

3.5. PHL influences the alterations in myocardial mitochondrial ultrastructure

As shown in Fig. 7, the images revealed that the myocardium mitochondria had an ordinary morphological structure in the CONT group. However, most of the myocardium mitochondria in the ISO group were blackened, the mitochondria were swollen, the crest was short or dissolved, the cristae vanished, and the mitochondria appeared vesiculiform. These events revealed that PHL treatment hindered the evolution of mitochondrial injury.

3.6. PHL effects on the level of apoptosis-related proteins in MF mice

The changes in the apoptosis-related proteins Bax (Fig. 8B), Bcl-2 (Fig. 8C), and Caspase-3 (Fig. 8D) in myocardial tissues were detected, and it was found that the expression of Bax and Caspase-3 in the ISO group was greater than that in the CONT group ($p < 0.01$), whereas the Bcl-2 level was lower ($p < 0.01$). Additionally, PHL treatment effectively downregulated Bax and Caspase-3 and upregulated Bcl-2 ($p < 0.01$ or $p < 0.05$, respectively) (Fig. 8A).

3.7. PHL downregulates the expression of inflammatory factors in MF mice

The protein expression of the inflammatory factors TNF-α, IL-1β, and IL-18 (Fig. 9A–C) in the cardiac tissue of mice was examined in each group. Compared to that in the CONT group, the protein expression of the inflammatory factors TNF-α, IL-1β, and IL-18 in the ISO group was observably elevated ($p < 0.01$), whereas PHL treatment effectively decreased the expression of inflammatory factors (p
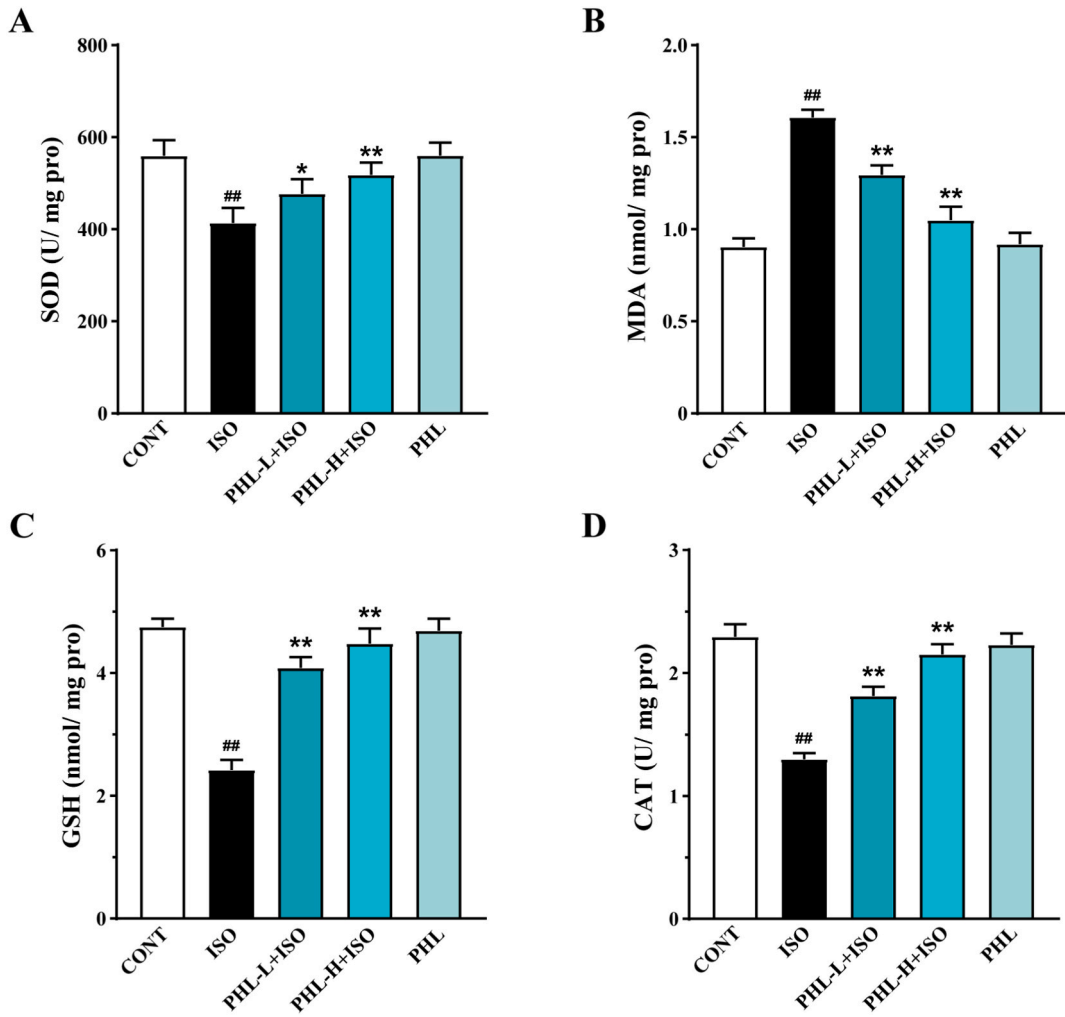
Fig. 5. Expression of SOD (A), MDA (B), GSH (C) and CAT (D) are shown between the ISO group and PHL treatment groups. Data are shown as the mean ± SEM (n = 6). ##$p < 0.01$ vs. CONT group; **$p < 0.01$, *$p < 0.05$ vs. ISO group.
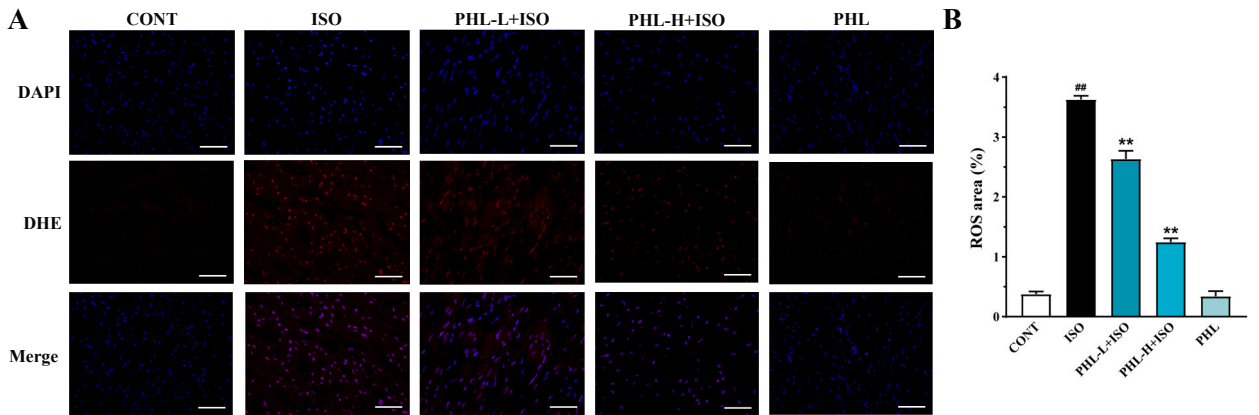

Fig. 6. Changes in ROS expression in ISO-induced mice induced by PHL. (A) Representative ROS leaves from the CONT, ISO, PHL-L + ISO, PHL-H + ISO, and PHL groups (scale bar: 50 μm). (B) ROS fluorescent area. Data are shown as the mean ± SEM (n = 3). ##$p < 0.01$ vs. CONT group; **$p < 0.01$ vs. ISO group.
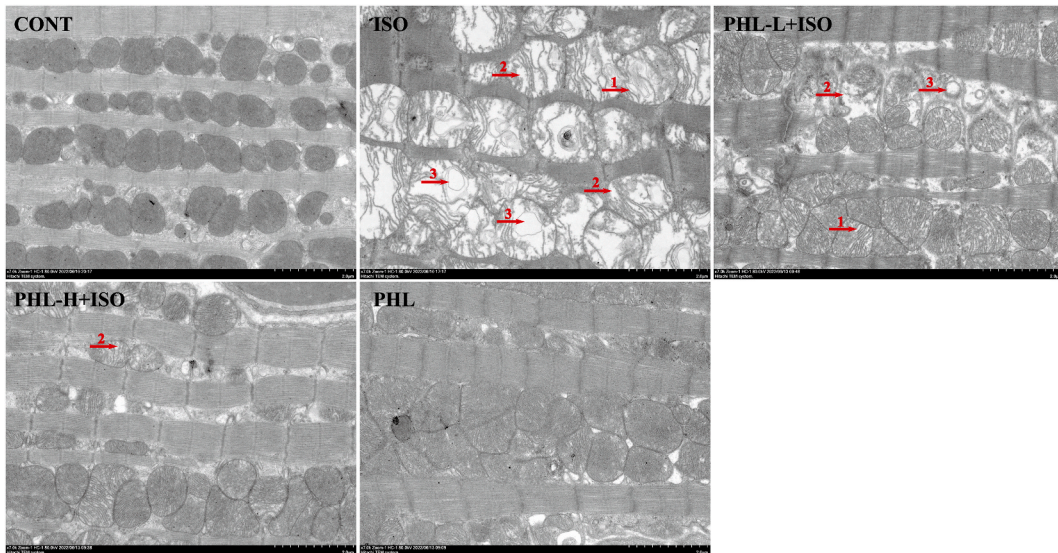
Fig. 7. Modifications in myocardium mitochondrion ultrastructure between the ISO group and PHL treatment groups (scale bar: 2.0 μm, magnification: 7.0k ×). These figures represent the CONT, ISO, PHL-L + ISO, PHL-H + ISO, and PHL groups, respectively. TEM images revealed ultrastructural alterations of myocardial mitochondria: the mitochondria were swollen, and the cristal space was enlarged (arrow 1), the crest became short or dissolved (arrow 2), the cristae vanished, and the mitochondria appeared vesiculiform (arrow 3).

< 0.01). These issues indicated that PHL could restrain the inflammatory level of MF mice.

3.8. PHL attenuates ISO-induced MF by regulating the HK1/NLRP3 pathway to inhibit pyroptosis

Western blotting was applied to examine the protein expression of HK1 (Fig. 10B), NLRP3 (Fig. 10C), ASC (Fig. 10D), Caspase-1 (Fig. 10E), and GSDMD-N (Fig. 10G). Compared with that in the CONT group, the protein expression of HK1, NLRP3, ASC, Caspase-1, and GSDMD-N in the ISO group was visibly upregulated ($p < 0.01$), and PHL treatment obviously downregulated their expression ($p < 0.01$, $p < 0.05$), suggesting that PHL restrained the activation of the NLRP3 inflammasome in MF mice (Fig. 10A and F). These results confirmed that PHL could enhance MF by restraining the HK1 pathway and restraining the stimulation of the NLRP3 inflammasome.

4. Discussion

MF, a morphological feature of ventricular remodeling, is a universal pathological manifestation of various heart diseases. When the collagen ratio is imbalanced, a fibrotic scar replaces the damaged tissue, and the intercellular substance dilates, promoting MF. The extracellular matrix is deposited excessively in the myocardium, which increases the stiffness of the ventricular wall, leading to the impairment of cardiac diastolic dysfunction [24]. MF is a typical complication of long-term unfavorable prognosis in MI patients and compensatory response to myocardium impairments. In preclinical studies, ISO is an extensively applied inducer for MI at a certain high dose, and it has presented morphological distortion in experimental animal tissues.

Oxidative stress can promote MF by directly activating the proliferation of cardiac fibroblasts or indirectly participating in the signal transduction of cytokines and growth factors through ROS [25,26]. SOD, GSH and CAT are the first lines of defense against oxidative damage, and MDA is the resulting product of the peroxidation reaction between ROS and lipids and is detected as a sign of oxidative stress [27]. Consistent with previous findings, ISO induced significant oxidative stress in myocardial tissue in this study, mainly via the production of a large amount of ROS (Fig. 6) and MDA and a marked decrease in the activities of SOD, CAT, and GSH. Meanwhile, PHL treatment alleviated oxidative stress by balancing the activity of antioxidant systems, ROS production and MDA levels. It was suggested that PHL has obvious antioxidant activity in these findings.

The accumulation of ROS in mitochondria oxidizes macromolecular proteins and DNA structures and then destroys the mitochondrial structure, resulting in increased mitochondrial membrane permeability [28]. TEM images showed the ultrastructure differences of ISO-induced myocardium mitochondria: mitochondrial swelling, cristal space expansion, cristae disappearance, vesicular mitochondria and an enlarged or broken space between myofilaments. However, after treatment with PHL, the morphology and integrity of mitochondria were significantly improved (Fig. 7).

The mitochondrial signaling pathway is a classic apoptotic signal. When the mitochondrial permeability transition pore opens, cytochrome C escapes into the cytoplasm and activates the apoptotic pathway to cause cardiomyocyte apoptosis [29]. Both the proapoptotic protein Bax and the antiapoptotic protein Bcl-2 belong to the Bcl-2 protein family. When stimulated by apoptotic signals, Bax is transferred from the cytoplasm to the mitochondria, binds to the mitochondrial membrane, and then antagonizes Bcl-2 located on the mitochondrial membrane to play a proapoptotic role. Activating Caspase-3 will ultimately result in apoptosis because Caspase-3
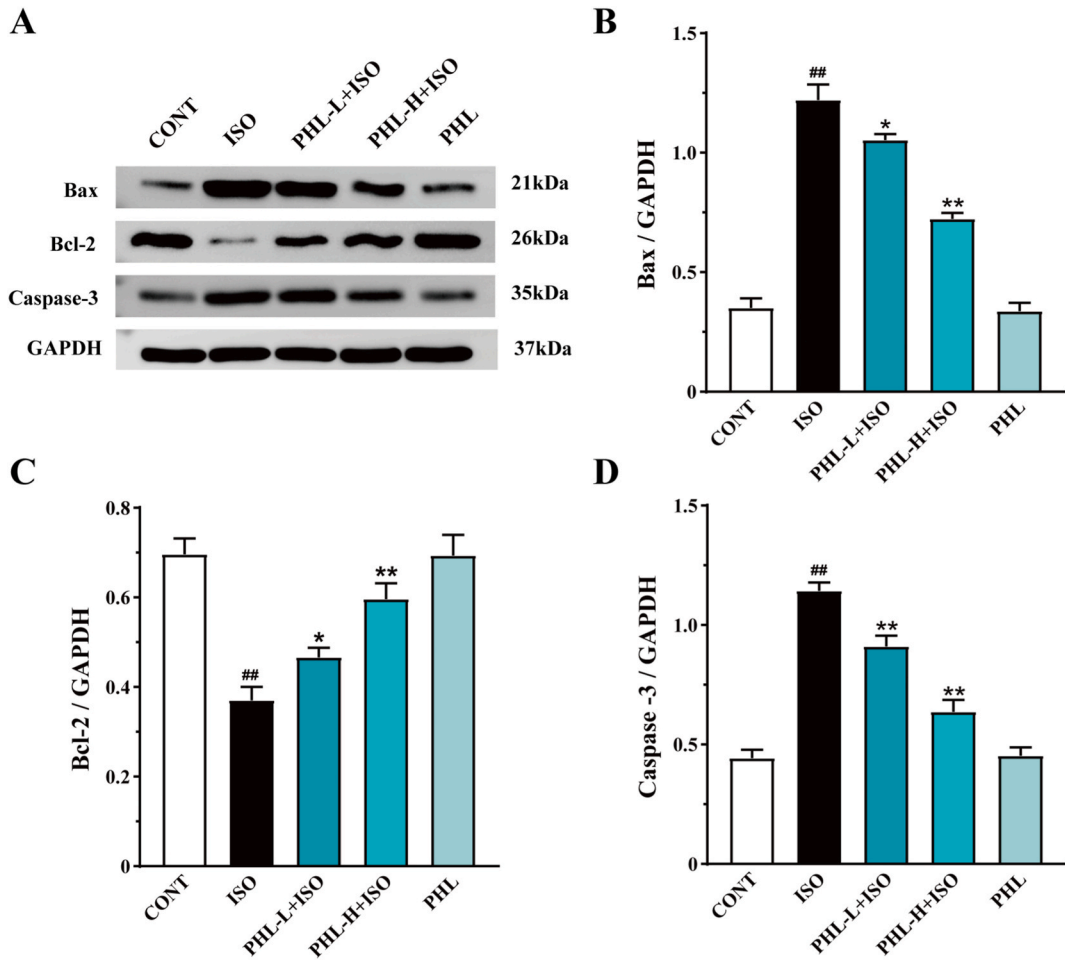
Fig. 8. The effects of PHL on expression of the apoptosis factors Bax (B), Bcl-2 (C), and Caspase-3 (D) in ISO-induced mice (A). Data are shown as the mean ± SEM (n = 3). ##$p < 0.01$ vs. CONT group; **$p < 0.01$, *$p < 0.05$ vs. ISO group.
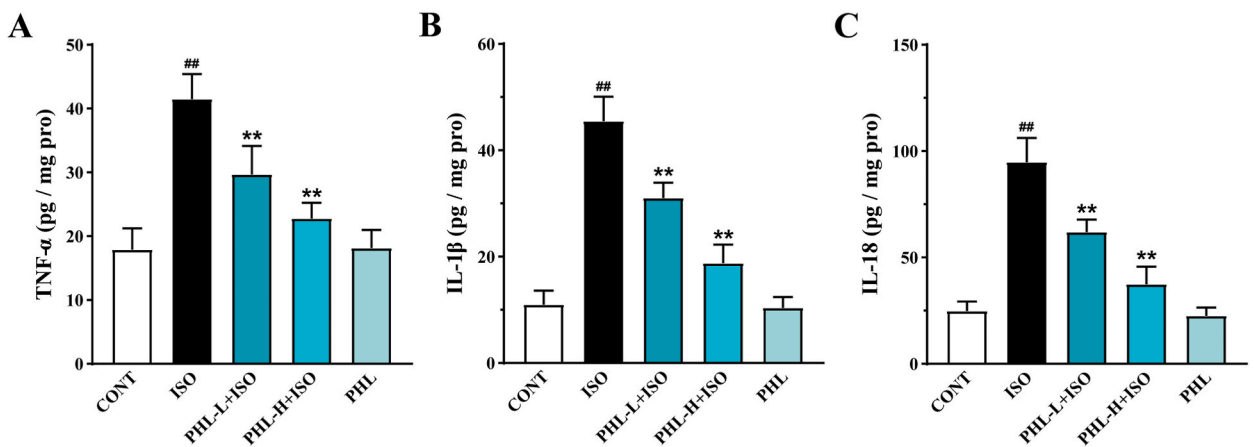

Fig. 9. The effects of PHL on expression of the inflammatory cytokines TNF-α (A), IL-1β (B) and IL-18 (C) in ISO-induced mice. Data are shown as the mean ± SEM (n = 6). ##$p < 0.01$ vs. the CONT group; **$p < 0.01$ vs. the ISO group.
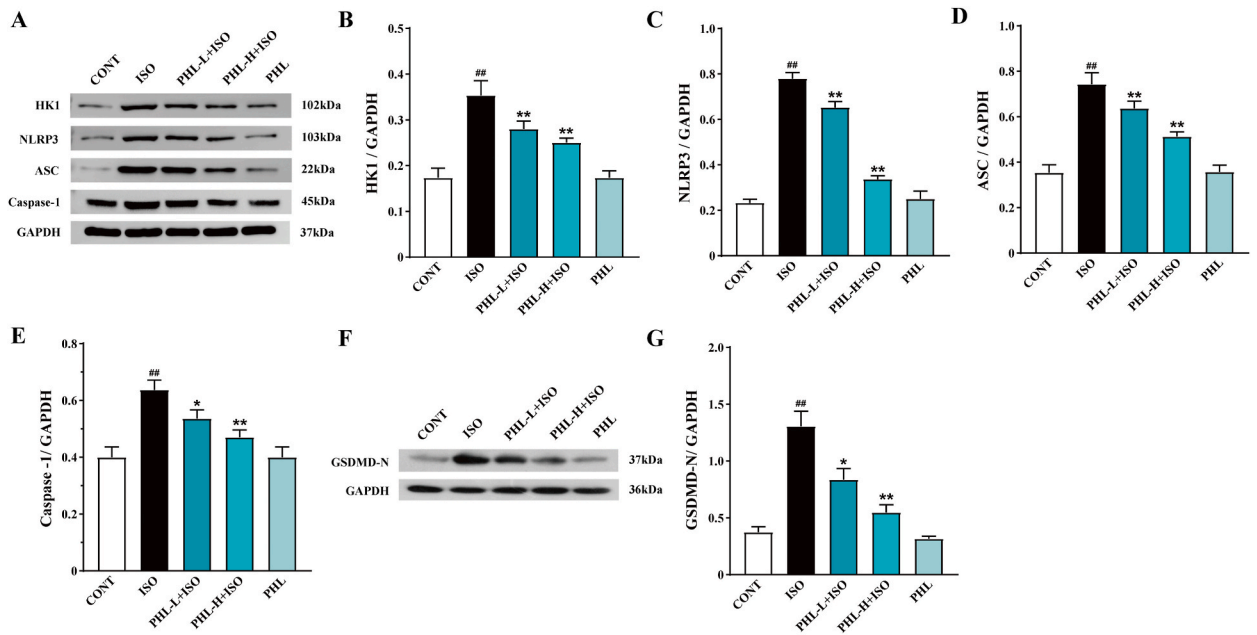
Fig. 10. The effects of PHL on expression of the signal pathway proteins HK1 (B), NLRP3 (C), ASC (D), Caspase-1 (E), and GSDMD-N (G) in ISO-induced mice (A and F). Data are shown as the mean ± SEM (n = 3). ##$p < 0.01$ vs. CONT group; **$p < 0.01$, *$p < 0.05$ vs. ISO group.

is the critical bridge builder of the apoptosis signaling pathway [30]. Western blot results revealed that Bax and Caspase-3 expression levels were observably increased in the ISO group, and Bcl-2 expression levels were significantly decreased in the ISO group. However, after PHL treatment, Bax and Caspase-3 expression was markedly reduced, and Bcl-2 expression was markedly increased (Fig. 8). Therefore, PHL may improve the degree of MF by inhibiting apoptosis.

Excessive ROS production causes mitochondrial dysfunction accompanied by stimulation of the NLRP3 inflammasome [31], the latter of which plays a significant role in myocardial scar formation and remodeling [32]. In response to inflammatory reactions, proinflammatory mediators are released, and the infiltration of inflammatory cells is increased. Vincristine mediates the down-regulation of Caspase-1, IL-1β, and IL-18, which reduces cardiac fibrosis by directly inhibiting stimulation of the NLRP3 inflammasome [33]. It is worth noting that pyroptosis is also referenced in the regulation of cardiovascular condition development, including MF [34], and the NLRP3/Caspase-1 signaling pathway is the classical pathway. GSDMD, as a pyroptosis effitor, can be cleaved into GSDMD-N by activating Caspase-1, which binds to the cell membrane and oligomerizes to form pores [35]. Then, pyroptosis induces inflammation by releasing proinflammatory cytokines such as IL-1β and IL-18 through the pore [36].

Research by Li [37] provided evidence that a Caspase-1 inhibitor can significantly inhibit vascular smooth muscle cell pyroptosis in atherosclerosis by suppressing NLRP3-mediated pyroptosis. HK1 plays a key role in glucose homeostasis and energy metabolism mediated by glucose phosphorylation or glucose signal transduction. The inhibition of HK1 leads to a decrease in glycolysis, thereby suppressing the generation of IL-1β and the stimulation of Caspase-1 in response to lipopolysaccharide [14]. In this study, the levels of HK1, NLRP3, ASC, Caspase-1 and GSDMD-N were markedly increased in the ISO group, whereas PHL treatment effectively down-regulated the expression of HK1, NLRP3, ASC, Caspase-1 and GSDMD-N (Fig. 10). Our results suggest that PHL can downregulate the level of cardiomyocyte pyroptosis by inhibiting the rate-limiting enzyme HK1 in glycolysis. Therefore, among the mechanisms regulating pyroptosis, the HK1/NLRP3 pathway is considered an anti-pyroptosis defense mechanism, and PHL may be an effective drug to protect against MF by antipyroptosis in future clinical practice (Fig. 11).

5. Conclusion

In summary, PHL protected against ISO-induced MF through antioxidative stress, alleviating mitochondrial damage, anti-apoptosis, and anti-pyroptosis, and may inhibit pyroptosis by regulating the HK1/NLRP3 signaling pathway *in vivo*.

Ethics statement

The animal study was reviewed and approved by the Institutional Animal Care and Use Committee of the Hebei University of Chinese Medicine.
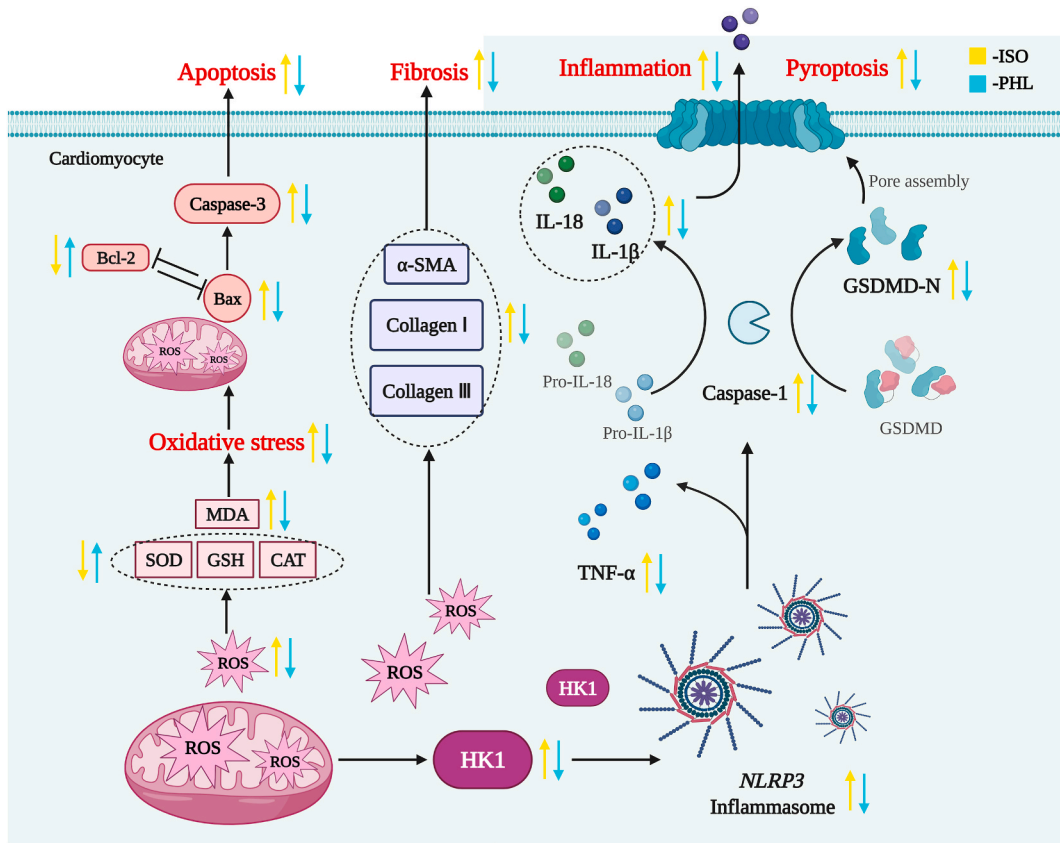
Fig. 11. Mechanism for the protective effects of PHL against ISO-induced myocardial fibrosis (MF).

Author contribution statement

Yuling Zhang: Conceived and designed the experiments; Performed the experiments; Analyzed and interpreted the data; wrote the paper. Xizhen Cheng: Performed the experiments; Analyzed and interpreted the data; Wrote the paper. Yanan Wang: Performed the experiments; Analyzed and interpreted the data. Haochuan Guo: Contributed reagents, materials, analysis tools or data. Yongxing Song, Hongfang Wang, and Donglai Ma: Conceived and designed the experiments; Analyzed and interpreted the data; Wrote the paper.

Funding statement

Data availability statement

Data will be made available on request.

Declaration of competing interest

The authors declare that they have no known competing financial interests or personal relationships that could have appeared to influence the work reported in this paper.

References

[1] M. Bouvet, O. Claude, M. Roux, D. Skelly, N. Masurkar, N. Mougenot, et al., Anti-integrin αv therapy improves cardiac fibrosis after myocardial infarction by blunting cardiac PW1+ stromal cells, Sci Rep-UK 10 (1) (2020), 11404.

[2] S. Park, N.B. Nguyen, A. Pezhouman, R. Ardehali, Cardiac fibrosis: potential therapeutic targets, Transl. Res. 209 (2019) 121–137.

[3] S. Sun, A. Dawuti, D. Gong, R. Wang, T. Yuan, S. Wang, et al., Puerarin-V improve mitochondrial respiration and cardiac function in a rat model of diabetic cardiomyopathy via inhibiting pyroptosis pathway through P2X7 receptors, Int. J. Mol. Sci. 23 (21) (2022), 13015.

[4] A. Kazakov, R.A. Hall, C. Werner, T. Meier, A. Trouvain, S. Rodionycheva, et al., Raf kinase inhibitor protein mediates myocardial fibrosis under conditions of enhanced myocardial oxidative stress, Basic Res. Cardiol. 113 (6) (2018) 42.

[5] J. Luo, D. Yan, S. Li, S. Liu, F. Zeng, C.W. Cheung, et al., Allopurinol reduces oxidative stress and activates Nrf2/p62 to attenuate diabetic cardiomyopathy in rats, J. Cell Mol. Med. 24 (2) (2020) 1760–1773.

[6] I. Rahim, R.K. Sayed, M. Fernández-Ortiz, P. Aranda-Martínez, A. Guerra-Librero, J. Fernández-Martínez, et al., Melatonin alleviates sepsis-induced heart injury through activating the Nrf2 pathway and inhibiting the NLRP3 inflammasome, N-S Arch Pharmacol. 394 (2) (2021) 261–277.

[7] Y. Li, P. Liang, B. Jiang, Y. Tang, Q. Lv, H. Hao, et al., CARD9 inhibits mitochondria-dependent apoptosis of cardiomyocytes under oxidative stress via interacting with Apaf-1, Free Radical Biol. Med. 141 (2019) 172–181.

[8] J.F. Peng, X.N. Zhao, M. Zhang, J.Y. Li, C.C. Zhao, S.S. Wang, et al., Punicalagin attenuates ventricular remodeling after acute myocardial infarction via regulating the NLRP3/caspase-1 pathway, Pharm. Biol. 61 (1) (2023) 963–972.

[9] R. Yue, Z. Zheng, Y. Luo, W. Wang, M. Lv, D. Qin, et al., NLRP3-mediated pyroptosis aggravates pressure overload-induced cardiac hypertrophy, fibrosis, and dysfunction in mice: cardioprotective role of irisin, Cell Death Dis. 7 (1) (2021) 50.

[10] A. Li, Y. Yu, X. Ding, Y. Qin, Y. Jiang, X. Wang, et al., MiR-135b protects cardiomyocytes from infarction through restraining the NLRP3/caspase-1/IL-1β pathway, Int. J. Cardiol. 307 (2020) 137–145.

[11] J. Chen, M. Pan, J. Wang, M. Zhang, M. Feng, X. Chai, et al., Hydroxysafflor yellow A protects against colitis in mice by suppressing pyroptosis via inhibiting HK1/NLRP3/GSDMD and modulating gut microbiota, Toxicol. Appl. Pharmacol. 467 (2023), 116494.

[12] C.R. Amendola, J.P. Mahaffey, S.J. Parker, I.M. Ahearn, W.C. Chen, M. Zhou, et al., KRAS4A directly regulates hexokinase 1, Nature 576 (7787) (2019) 482–486.

[13] Y. Qian, D. Chen, Y. Zhu, J. Wu, Y. Wang, W. Yang, Targeting hexokinase 1 alleviates NLRP3-mediated inflammation in apical periodontitis: a laboratory investigation, Int. Endod. J. 56 (6) (2023) 734–747.

[14] H. Jin, Y. Zhu, X.D. Wang, E.F. Luo, Y.P. Li, B.L. Wang, Y.F. Chen, Bdnf corrects NLRP3 inflammasome-induced pyroptosis and glucose metabolism reprograming through KLF2/HK1 pathway in vascular endothelial cells, Cell. Signal. 78 (2021), 109843.

[15] L. Cardoso-Sousa, E.M.G. Aguiar, D.C. Caixeta, D.D. Vilela, D.P.D. Costa, T.L. Silva, et al., Effects of salbutamol and phlorizin on acute pulmonary inflammation and disease severity in experimental sepsis, PLoS One 14 (9) (2019), e0222575.

[16] Z. Jia, Y. Xie, H. Wu, Z. Wang, A. Li, Z. Li, et al., Phlorizin from sweet tea inhibits the progress of esophageal cancer by antagonizing the JAK2/STAT3 signaling pathway, Oncol. Rep. 46 (1) (2021) 8088.

[17] F. Liu, X. Wang, Y. Cui, Y. Yin, D. Qiu, S. Li, X. Li, Apple polyphenols extract (APE) alleviated dextran sulfate sodium induced acute ulcerative colitis and accompanying neuroinflammation via inhibition of apoptosis and pyroptosis, Foods 10 (11) (2021) 2711.

[18] M. Hirose, T. Shibazaki, T. Nakada, T. Kashihara, S. Yano, Y. Okamoto, et al., Phlorizin prevents electrically-induced ventricular tachyarrhythmia during ischemia in langendorff-perfused Guinea-pig hearts, Biol. Pharm. Bull. 37 (7) (2014) 1168–1176.

[19] Q. Cai, B. Li, F. Yu, W. Lu, Z. Zhang, M. Yin, H. Gao, Investigation of the protective effects of phlorizin on diabetic cardiomyopathy in db/db mice by quantitative proteomics, J. Diabetes Res. 2013 (2013), 263845.

[20] H.N. Althurwi, M.S. Abdel-Kader, K.M. Alharthy, M.A. Salkini, F.F. Albaqami, Cymbopogon proximus essential oil protects rats against isoproterenol-induced cardiac hypertrophy and fibrosis, Molecules 25 (8) (2020) 1786.

[21] T. Zhao, H.J. Kee, L. Bai, M.K. Kim, S.J. Kee, M.H. Jeong, Selective HDAC8 inhibition attenuates isoproterenol-induced cardiac hypertrophy and fibrosis via p38 mapk pathway, Front. Pharmacol. 12 (2021), 677757.

[22] L. Shi, X. Du, B. Zuo, J. Hu, W. Cao, Qige huxin formula attenuates isoprenaline-induced cardiac fibrosis in mice via modulating gut microbiota and protecting intestinal integrity, Evid-Based Compl Alt 2022 (2022), 2894659.

[23] W. Zhang, S. Chen, H. Fu, G. Shu, H. Tang, X. Zhao, et al., Hypoglycemic and hypolipidemic activities of phlorizin from Lithocarpus polystachyus rehd in diabetes rats, Food Sci. Nutr. 9 (4) (2021) 1989–1996.

[24] S.K. Hong, E.H. Choo, S.H. Ihm, K. Chang, K.B. Seung, Dipeptidyl peptidase 4 inhibitor attenuates obesity-induced myocardial fibrosis by inhibiting transforming growth factor-βl and Smad2/3 pathways in high-fat diet-induced obesity rat model, Metabolism 76 (2017) 42–55.

[25] A.Y. Li, J.J. Wang, S.C. Yang, Y.S. Zhao, J.R. Li, Y. Liu, et al., Protective role of gentianella acuta on isoprenaline induced myocardial fibrosis in rats via inhibition of NF-κB pathway, Biomed. Pharmacother. 110 (2019) 733–741.

[26] P. Lin, X. Tong, F. Xue, C. Qianru, T. Xinyu, L. Zhe, et al., Polystyrene nanoplastics exacerbate lipopolysaccharide-induced myocardial fibrosis and autophagy in mice via ROS/TGF-β1/Smad, Toxicology 480 (2022), 153338.

[27] L.L. Kang, D.M. Zhang, R.Q. Jiao, S.M. Pan, X.J. Zhao, Y.J. Zheng, et al., Pterostilbene attenuates fructose-induced myocardial fibrosis by inhibiting ROS-Driven Pitx2c/miR-15b pathway, Oxid Med Cell Ongev 2019 (2019), 1243215.

[28] H. He, L. Wang, Y. Qiao, Q. Zhou, H. Li, S. Chen, et al., Doxorubicin induces endotheliotoxicity and mitochondrial dysfunction via ROS/eNOS/NO pathway, Front. Pharmacol. 10 (2019) 1531.

[29] H.A. Kalpage, V. Bazylianska, M.A. Recanati, A. Fite, J. Liu, J. Wan, et al., Tissue-specific regulation of cytochrome C by post-translational modifications: respiration, the mitochondrial membrane potential, ROS, and apoptosis, Faseb. J. : official publication of the Federation of American Societies for Experimental Biology 33 (2) (2019) 1540–1553.

[30] A. Iqubal, S. Sharma, M.A. Ansari, A.K. Najmi, M.A. Syed, J. Ali, et al., Nerolidol attenuates cyclophosphamide-induced cardiac inflammation, apoptosis and fibrosis in Swiss Albino mice, Eur. J. Pharmacol. 863 (2019), 172666.

[31] S. Wei, W. Ma, X. Li, C. Jiang, T. Sun, Y. Li, et al., Involvement of ROS/NLRP3 inflammasome signaling pathway in doxorubicin-induced cardiotoxicity, Cardiovasc. Toxicol. 20 (5) (2020) 507–519.

[32] X. Li, J. Geng, J. Zhao, Q. Ni, C. Zhao, Y. Zheng, et al., Trimethylamine N-oxide exacerbates cardiac fibrosis via activating the NLRP3 inflammasome, Front. Physiol. 10 (2019), 00866.

[33] C. Ge, Y. Cheng, Y. Fan, Y. He, Vincristine attenuates cardiac fibrosis through the inhibition of NLRP3 inflammasome activation, Clin. Sci. (Lond.) 135 (11) (2021) 1409–1426.

[34] J. Wang, B. Deng, Q. Liu, Y. Huang, W. Chen, J. Li, et al., Pyroptosis and ferroptosis induced by mixed lineage kinase 3 (MLK3) signaling in cardiomyocytes are essential for myocardial fibrosis in response to pressure overload, Cell Death Dis. 11 (7) (2020) 574.

[35] X. Wu, H. Zhang, W. Qi, Y. Zhang, J. Li, Z. Li, et al., Nicotine promotes atherosclerosis via ROS-NLRP3-mediated endothelial cell pyroptosis, Cell Death Dis. 9 (2) (2018) 171.

[36] M.B. Sordi, L. Panahipour, Z. Kargarpour, R. Gruber, Platelet-rich fibrin reduces IL-1&β; release from macrophages undergoing pyroptosis, Int. J. Mol. Sci. 23 (15) (2022) 8306.

[37] Y. Li, X. Niu, H. Xu, Q. Li, L. Meng, M. He, et al., VX-765 attenuates atherosclerosis in ApoE deficient mice by modulating VSMCs pyroptosis, Exp. Cell Res. 389 (1) (2020) 111847.